New Phase and Frequency Detectors for Carrier Recovery in PSK and QAM Systems

HIKMET SARI, MEMBER, IEEE, AND SAÏD MORIDI

Abstract—**New phase and frequency detectors (PFD's) are presented that considerably extend the acquisition range of carrier recovery loops in digital communication systems. Based on a simple modification of conventional phase detectors (PD's), the new detectors are applicable to a large variety of modulation schemes including the popular PSK and QAM signal formats. Their application to QPSK, 16 and 64 QAM, is extensively discussed, and simulated frequency detector (FD) characteristics as well as acquisition behavior of several PFD's are reported for QPSK and 16 QAM. The results of an experimental evaluation using a 16 QAM laboratory modem are also reported which show that the new detectors increase the acquisition range achievable by conventional PD's by more than on order of magnitude. In PSK, the improved acquisition performance is obtained with no penalty in steady-state phase jitter. In combined amplitude and phase shift keying, it generally leads to increased jitter, but this is easily avoided by incorporating a lock indicator and switching back to the original PD after lock is acquired.**

I. Introduction

CARRIER synchronization is a critical issue in many digital communication systems, and particularly, in digital microwave radio applications where the frequency offset can take large values due to the frequency uncertainty of the RF oscillators used in up- and down-conversion between the intermediate frequency (IF) and the carrier frequency. The bandwidth-efficient modulation techniques used in these systems, e.g., 16 and 64 QAM, are very sensitive to phase jitter and require very narrow loop bandwidths in carrier recovery. Typical loop bandwidths are below 10 kHz. The requirement of narrow loop bandwidth will be even more stringent in future radio systems employing 256 QAM [1], [2]. On the other hand, the frequency uncertainty of the RF oscillators lead to absolute frequency offsets that can attain several hundreds of kHz, and the carrier recovery loop must acquire lock in these conditions.

These two requirements, i.e., sufficiently small phase jitter and large acquisition (or pull-in) range, are not compatible in conventional phase locked loop (PLL) design. The common approach to overcome this difficulty is to design a narrow-band loop satisfying the phase jitter requirement, and to extend the acquisition range using some form of acquisition aiding techniques. Among various acquisition aiding techniques [3], we can mention the following:

a) switching of the loop filter,
b) use of a nonlinear element in the loop filter,
c) frequency sweeping, and
d) frequency detectors.

The first of these methods is based on using a large filter bandwidth during the acquisition process, and then switching to a narrow loop filter after lock is achieved. Obviously, the method requires a lock detector to control the switch. In the second method, a nonlinear element is inserted in the loop between the phase detector (PD) and the loop filter [4], or the loop filter itself comprises a nonlinear element. The basic idea is to make one of the loop parameters depend on the magnitude of the PD output so that the loop behavior changes as phase lock is achieved. A particular design in which the varying parameter is one of the loop time constants is described in [3], while the particular scheme described in [4] is based on varying the loop gain.

The most common acquisition aiding technique employed in digital microwave radio is frequency sweeping. This consists of sweeping the IF oscillator frequency over the uncertainty interval which can be done by adding to the filtered PD output a periodic signal (e.g., sinusoidal or triangular) until lock is acquired. Once phase lock is achieved, frequency sweeping is stopped to avoid an undesirable increase of the phase jitter. Although frequency sweeping is commonly employed, it has a serious limitation: the loop acquires lock with certainty only if the sweep rate is less than a maximum value, empirically given in [5] for sinusoidal PD's and high SNR's as $\omega_n/2$ where ω_n is the loop natural frequency. This constraint leads to slow acquisition, typically on the order of 100 ms in state-of-the-art digital radio systems.

Another acquisition aiding technique is the use of a frequency detector (FD), also called frequency difference detector. Conventional FD's are only useful for frequency acquisition, i.e., they cannot be used for phase acquisition and tracking. Therefore, an FD is traditionally used in parallel with a PD, and the respective outputs of the two are summed after separate filtering, as shown in Fig. 1. In this configuration, the loop acquisition behavior is governed by the FD during acquisition, and by the PD in the steady state. After lock is acquired, the FD gives essentially zero output and, consequently, does not increase the steady-state phase jitter. Frequency detectors of this type have been previously applied to timing recovery [6], [7], and Costas loop carrier recovery for biphase signals [8]. With exception of the rotational FD proposed by Messerschmitt [6], all of these FD's are suited for analog implementation. A well-known example of those conventional FD's is the quadricorrelator [9], [10]. For CW inputs, the quadricorrelator requires two mixers, each followed by a low-pass filter, to transform the received signal into the corresponding in-phase (I) and quadrature (Q) baseband components. The I component is then differentiated, and the resulting signal is multiplied by the Q components. The dc component of the multiplier output is proportional to the frequency difference between the incoming signal and the local oscillator.

In the present paper, we take a different approach and derive a class of phase and frequency detectors (PFD's) that

Paper approved by the Editor for Synchronization Systems and Techniques of the IEEE Communications Society. Manuscript received May 17, 1988; revised November 23, 1988. This work was supported in part by Centre National d'Etudes des Telecommunications (CNET) under Contract 84.1B.010/LAB. This paper was presented in part at the 1986 IEEE International Conference on Communications, Toronto, Ont., Canada, June 1986.

The authors are with Laboratoires d'Electronique et de Physique Appliquée (a member of Philips Research Organization), 94451 Limeil Brévannes Cedex, France.

IEEE Log Number 8822631.

0090-6778/88/0900-1035$01.00

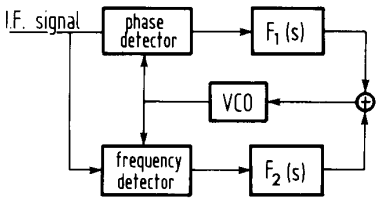

Fig. 1. Structure of a synchronization loop using an FD in parallel with the PD.

behave as frequency detectors during acquisition and phase detectors at steady state. They are obtained through a slight modification of conventional PD's, and only require very small additional circuitry. The new approach is applicable to carrier recovery in a large variety of modulation schemes. The philosophy of PFD's is, in fact, not completely new; some schemes were previously proposed by Cahn [8], and more recently by Vandamme *et al.* [11]. The former describes a modified Costas loop with a frequency discriminator characteristic applicable to biphase modulation, and the latter, a PFD based on detecting the zero crossings of the original PD characteristic (S curve), and most suited for PSK signals. Finally, although it does not consider PFD's, we mention here, for completeness, the survey paper by Natali [12] which summarizes the properties of eight different FD's.

The present paper is largely based on [13] in which we reported some preliminary results of the study. In the next section, we present the key idea behind the new PFD's, and explain how conventional PD's are easily transformed into PFD's. Specific schemes for carrier recovery in PSK and QAM systems are described in Section III. Characterization of these PFD's as well as their simulated acquisition performance are reported in Section IV. The following section reports on a laboratory experiment using a 16 QAM modem and several types of PFD's. Finally, in Section VI, we discuss some issues related to the loop steady-state jitter behavior.

II. Basic Principle

Although our main interest is in discrete-time PD's encountered in decision-feedback carrier recovery loops, we begin by considering a continuous-time PD and show how it can be transformed into an FD. We will focus on the sinusoidal PD to visualize the basic principle, but the approach is very general, and other PD's can be handled in a similar manner.

Fig. 2(a) shows the block diagram of an FD based on the new concept. The upper-arm PD of this structure is the PD that we transform into an FD by an appropriate manipulation of its output. Without any loss of generality, the two PD's that appear in this block diagram are assumed sinusoidal, and their output characteristics are sketched in Fig. 2(b) and (c), respectively. The lower-arm PD is in quadrature with the upper-arm PD, and therefore, its output characteristic is shifted by a quarter period with respect to that of the latter. The periodicity of $\pi/2$ assumed is that of a carrier recovery loop for rectangular QAM systems.

In the steady state, the phase error $\varphi(t)$ fluctuates around a stable lock point of the form $\Phi_k = k\pi/2$ where k is an integer. However, during acquisition, the phase error evolves at a speed that is proportional to the instantaneous frequency offset. To have a better view of this situation, assume that the loop is open and that the radian frequency offset is $\Delta\omega$. Then, the phase error evolves linearly with time as $\varphi(t) = \Delta\omega \cdot t + \varphi(0)$. The PD output is a sinusoidal signal of frequency $\Delta\omega$ that has a zero dc content. Stated in another way, in an open loop situation, the PD provides an output with zero dc, and hence, no information on the polarity of the frequency offset. In contrast, frequency detectors in a similar situation provide a

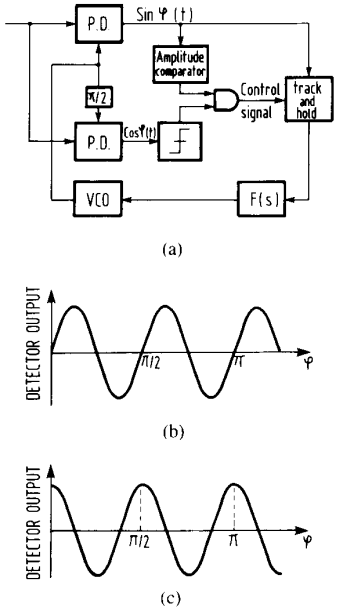

Fig. 2. (a) Block diagram of a PFD based on the new concept. (b) Main PD output characteristic. (c) Quadrature PD output (used as control signal).

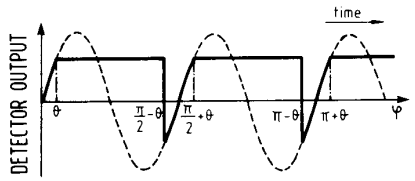

Fig. 3. Modified detector output in the presence of positive frequency offset.

dc output proportional to, or at least, having the same polarity as the frequency offset. Now, we show how the circuit of Fig. 2(a) performs an FD function.

The track-and-hold device in this figure is controlled in such a way that: a) it tracks the main (upper-arm) PD output when $|\varphi(t) - k\pi/2| < \theta$ with k integer and θ is an arbitrary angle ($\theta < \pi/4$), i.e., when the instantaneous phase error falls within an interval of width 2θ centered on a lock point $k\pi/2$, and b) it operates in a hold mode when the phase error is outside these intervals. More specifically, the track-and-hold device operates in a track mode when the amplitude of the main PD output is smaller than $\sin\theta$ and the quadrature PD output is positive. It switches to a hold mode as soon as one of these two conditions is not met. The control signal originating from the main PD output determines whether the phase error is within a predetermined interval centered on a transition point, and that originating from the quadrature PD output allows to recognize the stable lock points.

To view that this circuit performs an FD function, consider first a positive frequency offset. In this case, the phase error is an increasing function of time, and the track-and-hold device output describes the solid-line curve of Fig. 3. This curve coincides with the original PD output on each interval of the form $(k\pi/2 - \theta, k\pi/2 + \theta)$, but it is constant between two such intervals. With $\Delta\omega > 0$, the PD output at $\varphi = \theta$ is held in memory until $\varphi = \pi/2 - \theta$, its value at $\varphi = \pi/2 + \theta$ until $\varphi = \pi - \theta$, and so forth. Clearly, the track-and-hold device output has a positive dc.

Next, consider a negative frequency offset. In this case, the phase error being a decreasing function of time, it exits the

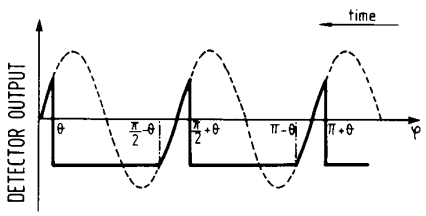

Fig. 4. Modified detector output in the presence of negative frequency offset.

intervals of interest, i.e., the $(k\pi/2 - \theta, k\pi/2 + \theta)$ intervals, at the points of the form $k\pi/2 - \theta$. Therefore, as shown in Fig. 4, the PD output at $\pi - \theta$ is memorized until $\pi/2 + \theta$, its output at $\pi/2 - \theta$ until θ, and so forth. Consequently, with $\Delta\omega < 0$, the track-and-hold device output has a negative dc.

Thus, by inserting an appropriately controlled track-and-hold device at the output of the sinusoidal PD, we have built an FD. Although we have focused on the sinusoidal PD, the method applied to any PD characteristic. In the absence of noise, the dc at the detector output is

$$\bar{v} = \left(1 - \frac{4\theta}{\pi}\right) g(\theta)\ \text{sgn}\ (\Delta\omega) \qquad (1)$$

where $g(\cdot)$ is the PD characteristic, assumed to be an odd function of φ.

At this point, two remarks are in order. First, it should be emphasized that the circuit that we have described is, in fact, a PFD. In the steady-state, the phase error $\varphi(t)$ remains small, the track-and-hold device remains in a track mode, and the loop behaves as in the case of the original PD. Therefore, the same circuit performs an FD function during acquisition, and a PD function during the steady state.

Second, the foregoing discussion focused on a continuous-time PD. Therefore, switching from the track mode to the hold mode occurred exactly at the points of the form $k\pi/2 + \theta$ for $\Delta\omega > 0$, and $k\pi/2 - \theta$ for $\Delta\omega < 0$. As will be seen in the next section, most carrier recovery loops of practical interest in PSK and QAM systems employ a discrete-time PD, and the phase error memorization process in these loops does not start exactly at these points. However, the described method still leads to an FD characteristic over a large range of the frequency offset.

Regarding the choice of θ, the optimum value is that which maximizes the dc at the detector output. This value depends on the original PD characteristic. As shown in Fig. 5, the optimum value of θ is approximately 16° for a sinusoidal PD and 22° for a sawtooth PD. These optimum values are valid only for continuous-time PD's for which the PFD resulting from the transformation has (in the absence of noise) a rectangular FD characteristic. For discrete-time PD's, even in the absence of noise, the FD characteristic is not rectangular, and the given θ values maximize the dc output only for small frequency offsets which is of no significant interest. The choice of θ in the case of discrete-time PD's and its influence on loop performance will be further discussed in Section IV.

III. Application to Carrier Recovery

The principle described in the previous section will be applied here to carrier recovery in PSK and QAM signal sets. In PSK, Nth power loops (N being the number of points in the signal constellation) and Costas loops [5] can be employed that are based on a continuous-time PD. However, in QAM systems, frequency multiplication cannot completely remove phase modulation of the signal, and most appropriate loops employ decision feedback. That is, phase information is extracted at the sampling instants from the detected data and the demodulated (and possibly equalized) signal. The discrete-time phase information is then filtered and fed to the VCO. A variety of such decision-feedback loops (DFL's) are described in [14]–[16]. In the sequel, we exclusively consider DFL's for their practical importance in carrier recovery.

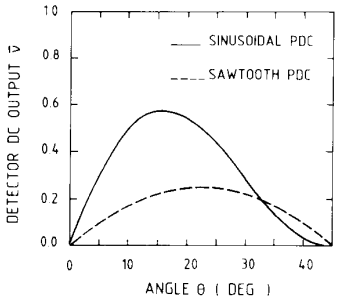

Fig. 5. Continuous-time PFD output versus angle θ for two types of PD.

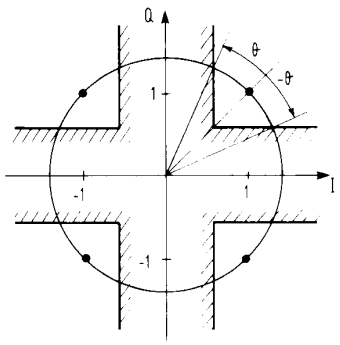

Fig. 6. PFD construction for carrier recovery in QPSK.

In PSK, transformation of a PD into a PFD according to the described principle is straightforward. The signal states are equispaced on a circle, and describe that circle in case of sync loss, as shown in Fig. 5 for the QPSK signal constellation. To derive a PFD, the PD output is activated and passed to the loop filter only when the demodulated signal point corresponds to an instantaneous phase error smaller than θ in magnitude. Otherwise, the previous output of the (discrete-time) PD is used as current input to the loop filter. Implementation of this concept requires: a) the design of appropriate windows placed around the nominal points of the signal constellation, and b) a control logic to test, at each sampling instant, whether the demodulated signal sample falls within one of these windows. The particular window design with vertical and horizontal boundaries shown in Fig. 6 has the advantage of implementation simplicity. With $(\pm 1 \pm j)$ being the four possible values of the complex symbols and with the window boundaries set at a distance of 0.5 from the horizontal and vertical axes, the angle θ is roughly 24°.

This principle is easily generalized to 8PSK and higher level PSK, but combined amplitude and phase shift-keying signal formats, such as rectangular QAM, require particular attention. In 16 QAM, the signal points describe three circles in case of sync loss. This is what a human observer would see on an oscilloscope when the carrier of the 16 QAM receiver is not synchronized with that of the transmitter. On the inner as well as on the outer circle, we can distinguish (Fig. 7) four equispaced signal points forming a QPSK signal set. On the middle circle, in contrast, there are (nonregularly spaced) 8 points which lead to phase ambiguity. To be more specific, upon reception of a signal point on the inner or the outer circle, the phase error (modulo $\pi/2$) can be exactly determined whereas with the points on the middle circle, a phase error φ cannot be distinguished from $\varphi + 36.9°$ or from $\varphi + 53.1°$.

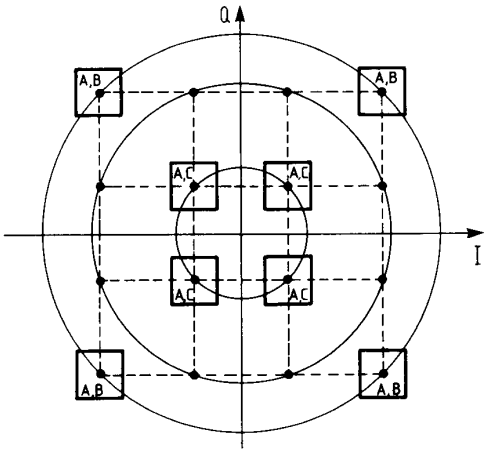

Fig. 7. PFD construction for carrier recovery in 16 QAM.

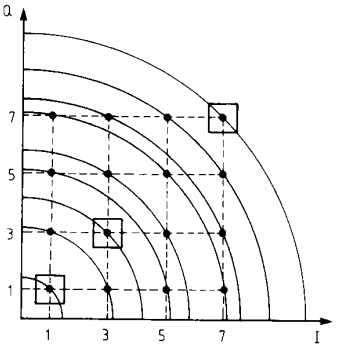

Fig. 8. PFD construction for carrier recovery in 64 QAM.

For this reason, the nondiagonal points are discarded in carrier recovery, some windows are drawn around the diagonal points, and the measured phase error is fed to the loop filter only when the received signal point falls within one of these windows. The previous PD output is held in memory and used as the current input to the loop filter otherwise. Fig. 7 shows a particular design with square-shaped windows where we can also notice that the windows centered on the outer diagonal points do not intersect with the middle circle. The reason for this is that for some phase errors, the nondiagonal points fall within the decision regions of the outer diagonal points and this leads to misinterpretation of the instantaneous phase error.

Generalization of this strategy to 64 QAM is summarized in Fig. 8 where only one quarter of the signal constellation is shown for convenience. It is seen that in case of sync loss, the signal points describe nine circles, and that on only 3 of them, there are 4 regularly-spaced signal points. All other circles have a large number of signal points leading to possible phase error misinterpretation. Based on the same arguments as in 16 QAM, we discard all nondiagonal points but also one diagonal point in each quadrant of the signal constellation. Appropriate windows are then placed around the remaining 12 diagonal points, and the current PD output is enabled only when the received signal point is within one of these windows. Again, care must be taken to draw these windows so as not to intersect with other circles.

A general block diagram of the proposed PFD's is shown in Fig. 9. For convenience, it is assumed in this figure that the PD output is binary so that only one flip flop is required for memorization. More generally, there will be as many flip flops as parallel bits at the PD output. In conventional DFL's,

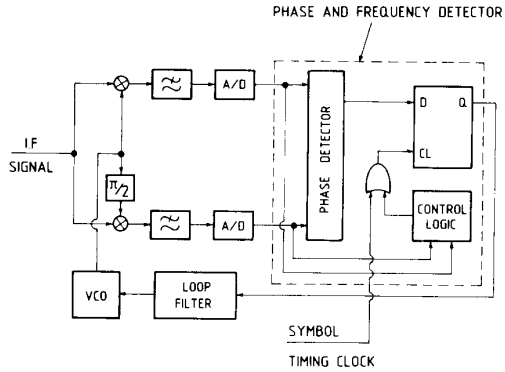

Fig. 9. General block diagram of carrier recovery loops employing the new PFD's.

the flip flops are controlled by the symbol timing clock; the only additional circuitry required by the proposed PFD's is the control logic that is used to cancel transitions of the timing clock when the demodulated signal sample is outside the predetermined windows.

The idea of using the current PD output when the demodulated signal sample is within some predetermined set of windows, and the previous output when the signal sample is outside this set can be found in [17]–[19]. However, this was done in a different context. Specifically, the goal was to use only the diagonal points of the 16 QAM signal constellation in carrier acquisition so as to avoid false phase locking. To this end, a control logic was used (as in Fig. 9) to determine whether the demodulated signal sample is within the decision region of the diagonal points of the signal constellation.

IV. FD Characteristics and Acquisition Behavior

We now illustrate the FD characteristics of the new detectors and then report their simulated acquisition performance. In all that follows, we assume a polarity-type decision-feedback phase detector [15], the output of which is

$$\epsilon_k = \text{sgn}\,(e_k^Q)\ \text{sgn}\,(I_k) - \text{sgn}\,(e_k^I)\ \text{sgn}\,(Q_k) \qquad (2)$$

with

$$e_k^I = I_k - \hat{a}_k$$

and

$$e_k^Q = Q_k - \hat{b}_k$$

where I_k and Q_k are the respective samples of the I and Q channels at the kth sampling instant, and $\hat{a}_k$ (resp. $\hat{b}_k$) is the detected data symbol whose detection is based on I_k (resp. Q_k). In (2), sgn(.) designates the mathematical sign function, i.e., $\text{sgn}(x) = 1$ for $x > 0$, and $\text{sgn}(x) = -1$ for $x < 0$. This phase detector is universal, i.e., it can be applied to any two-dimensional signal constellation.

A. Frequency Detector Characterization

The PFD derived from this PD, for QPSK, using the transformation described in Section III has the FD characteristic shown in Fig. 10, for the noiseless case and for an SNR of 20 dB, and for three distinct choices of the windows around the nominal signal points. Vertical and horizontal boundaries are used (as in Fig. 6), corresponding to $|I_k| > \alpha$ and $|Q_k| > \alpha$ where α is an arbitrary number between 0 and 1. A first observation is that for small frequency offsets, higher detector gains are achieved with larger values of α, which is in full agreement with (1) and the subsequent discussion (note that larger values of α correspond to smaller values of θ). In the

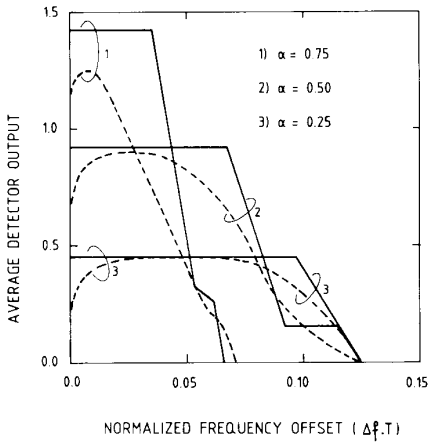

Fig. 10. FD characteristic of the new detectors in QPSK (—— noiseless case, ------ SNR = 20 dB).

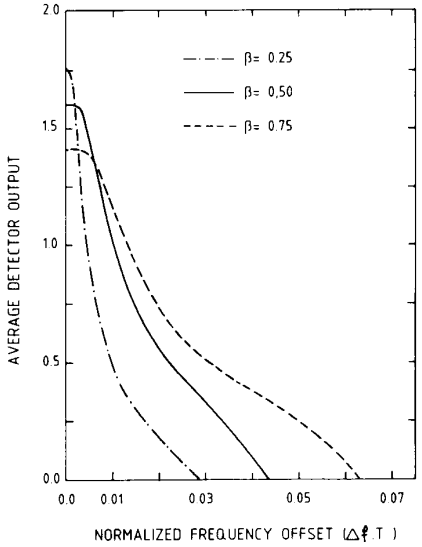

Fig. 11. FD characteristic of the new detectors in 16 QAM (SNR = 30 dB).

noiseless case, the FD characteristic is constant up to the frequency offset value given by

$$2\pi\Delta f \cdot T = \theta$$

where T is the symbol period, and θ the phase angle determined by the windows chosen. Beyond this value of Δf, the FD characteristic decreases rapidly due to the fact that evolution of the phase error over a symbol interval is higher than the angle θ, and the FD operation described in Section II no longer applies in a strict sense. The FD characteristic undergoes a sign change at some point after which acquisition is not possible. This value of the frequency offset constitutes an absolute limit on the acquisition range. Although the choice $\alpha = 0.75$ gives the highest detector gain for small Δf values, $\alpha = 0.25$ gives the largest frequency range over which the FD characteristic has the correct sign. This suggests that for small frequency offsets, faster acquisition should be achieved with $\alpha = 0.75$, but the acquisition range is larger with $\alpha = 0.25$, making this latter choice more attractive, since extention of the acquisition range is the primary goal. At the SNR of 20 dB, the useful frequency range is roughly the same as in the absence of noise, but the detector gain is smaller.

A similar characterization was made in the case of 16 QAM for two SNR's and three distinct choices of the windows. In the detectors considered, the PD output is used when the detected symbol is a diagonal point of the signal constellation with the additional requirement that $|e_k^I| < \beta$ and $|e_k^Q| < \beta$, for β some number less than 1. Fig. 11 shows the FD characteristics for SNR = 30 dB, and for three window choices given by $\beta = 0.25$, $\beta = 0.5$, and $\beta = 0.75$. The useful frequency range is evidently smaller than in QPSK, but this is not surprising, primarily because of the smaller phase angle used for the other diagonal points. In addition, even for small frequency offsets, the unused nondiagonal points in 16 QAM make it impossible to systematically start or stop the memorization process exactly when the value of the instantaneous phase error reaches θ or $-\theta$.

Computation of the FD characteristic can be done by Monte-Carlo techniques, but generation of long data sequences is needed to obtain sufficient averaging over the data symbols and the noise, as well as over the initial phase error. The required sequence length increases with the number of points in the signal constellation. Although, FD characterization in QPSK was done using a Monte-Carlo technique, the required sequence length is prohibitive in 16 QAM, and therefore, the following method was used instead.

Given the phase error value φ_n at instant n, the average open loop output can be computed as follows:

$$\bar{u}_n = E(\epsilon_n / r_n \in \mathfrak{D}) + p(r_n \notin \mathfrak{D})\bar{u}_{n-1}. \tag{4}$$

In this expression, $\bar{u}_{n-1}$ is the previous average PFD output conditional on φ_{n-1}, $p(r_n \notin \mathfrak{D})$ is the conditional probability that the instantaneous complex signal sample $r_k = I_k + jQ_k$ falls outside the set $\mathfrak{D}$ of the chosen windows, and finally, $E(\epsilon_n / r_n \in \mathfrak{D})$ is the average PD output ϵ_n conditional on φ_n and on r_n belonging to $\mathfrak{D}$. Note that (4) takes into account both additive noise (assumed to be Gaussian) and the fact that square windows are placed around some diagonal points only. In the simulation, starting from an initial phase error φ_o, the instantaneous phase error φ_n given by the frequency offset ($\varphi_n = 2\pi n.\ \Delta f.T + \varphi_o$) is calculated, and the average output at time n is computed using (4). Subsequent averaging is then made over the sequence n and over the initial phase error φ_o. This method was found to be considerably more accurate and more efficient than Monte-Carlo techniques.

B. Acquisition Performance

The next step of the study was the evaluation of the acquisition performance of the new PFD's and its comparison to the original phase detector. Unfortunately, an analytical evaluation of the acquisition range of PLL's comprising an FD does not seem feasible, and consequently, the evaluation was done by computer simulations.

A second-order loop with a phase lead-and-lag filter is assumed in the sequel. The Laplace transfer function of the filter is

$$F(s) = \frac{1 + \tau_2 s}{1 + \tau_1 s} \tag{5}$$

where τ_1 and τ_2 are two time constants which, together with the loop gain, determine the loop acquisition and steady-state properties.

The differential equation governing the phase error trajectory is

$$\dot{\varphi}(t) = \Omega - K_0 F(s) u(t) \tag{6}$$

where the dot designates time-derivative, Ω is the initial (radian) frequency offset, K_o is the VCO gain, and $u(t)$ is the continuous-time detector output. The mixed time domain and the Laplace transform domain variable notation used in (4) is

very common in the literature. The term $F(s)u(t)$ designates convolution of $u(t)$ with the impulse response of the loop filter. Making use of (5), (6) can be rewritten as a set of two differential equations

$$\dot{\varphi}(t) = X(t) - K_0 F_0 u(t) \tag{7.a}$$

and

$$X(t) = \Omega - \frac{K_0(1-F_0)}{1+\tau_1 s}\, u(t) \tag{7.b}$$

with $F_o = \tau_2/\tau_1$ (typically $F_o \ll 1$). In the DFL's at hand, the detector output $u(t)$ is constant over a symbol interval, i.e.,

$$u(t) = \Sigma u_k \text{ Rect } (t - kT) \tag{8}$$

with

$$\text{Rect } (t) = \begin{cases} 1, & 0 < t < T \\ 0, & \text{elsewhere.} \end{cases}$$

Solving (7.a) and (7.b) and making use of (8), we find the discrete-time difference equations

$$\varphi_{n+1} = \varphi_n + [\Omega - K_0(1-F_0)u_n]T + [X_n - \Omega + K_0(1-F_0)u_n] \cdot \tau_1(1 - e^{-T/\tau_1}) - K_0 T F_0 u_n \tag{9.a}$$

and

$$X_{n+1} = X_n + (1 - e^{-T/\tau_1})[\Omega - X_n - K_0(1-F_0)u_n]. \tag{9.b}$$

Finally, assuming $T/\tau_1 \ll 1$ for practical purposes, and making the change of variable $x_n = TX_n$ for convenience, (9.a) and (9.b) simplify to

$$\varphi_{n+1} \simeq \varphi_n + x_n - K_0 T F_0 u_n \tag{10.a}$$

and

$$x_{n+1} \simeq x_n + \frac{T}{\tau_1}[\Omega T - x_n - K_0 T(1-F_0)u_n]. \tag{10.b}$$

In the case of PLL's with a PD only, u_n is the PD output ϵ_n, but in the case of the PFD's at hand, the PFD output u_n is related to the PD output ϵ_n as

$$u_n = (1 - \chi_n)\epsilon_n + \chi_n u_{n-1} \tag{11}$$

and

$$\chi_n = \begin{cases} 0 & \text{if } r_n \in \mathfrak{D} \\ 1 & \text{otherwise.} \end{cases}$$

The set of difference equations (10.a) and (10.b) describes the evolution of the discrete-time stochastic phase error variable φ_n as well as of its low-frequency component x_n. The average phase trajectory is obtained by substituting for u_n in these equations its average value computed according to (4). The resulting pair of mean difference equations was used in our simulations to obtain the average acquisition time of the loop.

Using this method, the mean acquisition time was estimated and plotted as function of the frequency offset. This was done for both QPSK and 16 QAM and the three window choices mentioned previously. The results obtained using the loop parameters

$$W_L T = 8 \times 10^{-3} \quad (W_L\text{: two-sided loop noise bandwidth})$$

$$T/\tau_1 = 10^{-6}$$

and

$$\zeta = 0.707 \quad (\zeta\text{: damping factor})$$

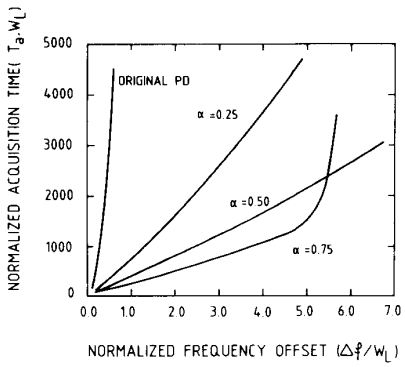

Fig. 12. Simulated acquisition time versus frequency offset in QPSK ($W_L T = 8 \times 10^{-3}$, $T/\tau_1 = 10^{-6}$, $\zeta = 0.707$).

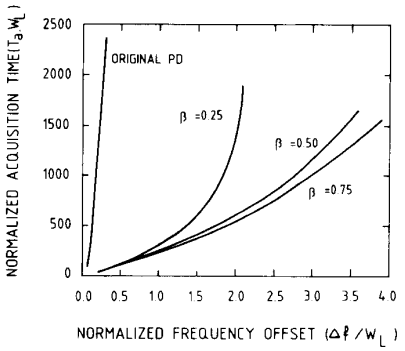

Fig. 13. Simulated acquisition time versus frequency offset in 16 QAM (same loop parameters as in Fig. 13, SNR = 30 dB).

are given in Fig. 12 for QPSK and in Fig. 13 for 16 QAM. In these figures, the frequency offset is normalized by the loop noise bandwidth W_L and the acquisition time by its inverse $1/W_L$.

Notice first that in both figures, the PFD's considered lead to a tremendous performance improvement with respect to the original PD, in terms of acquisition speed or acquisition range. Examining Fig. 12 further, we can also notice that over a large range of the frequency offset, the fastest acquisition among the three PFD's is achieved with the window choice $\alpha = 0.75$. It can be easily verified from this figure and Fig. 10 that this frequency range is precisely that over which the highest detector gain is obtained with $\alpha = 0.75$. Also, as predicted by the FD characteristics, the figure shows that $\alpha = 0.75$ leads to a smaller acquisition range than the other two α values. Over the frequency range shown in Fig. 12 (taking into account the noise bandwidth used in the simulations, $\Delta f/W_L = 7$ corresponds to $\Delta f.T = 0.056$), the figure also shows that $\alpha = 0.5$ leads to faster acquisition than $\alpha = 0.25$, which is in full agreement with the FD characteristics. Finally, the FD characteristics of Fig. 10 also suggest that these two values of the α parameter should lead to a similar acquisition range, but this could not be verified in simulation as it would take too much computer time.

In the case of 16 QAM (see Fig. 13), it is clear that the window choice $\beta = 0.25$ leads to the worst performance as it corresponds to a small phase angle particularly for the outer diagonal points of the signal constellation.

V. Experimental Evaluation

Acquisition performance of the new PFD's was also evaluated experimentally, using a 100 Mbit/s 16 QAM laboratory modem.

A. Description of the Experimental Setup

The 16 QAM modem used in the experiments employs raised-cosine Nyquist filtering with 50 percent excess bandwidth. At the receiver, the demodulated I and Q signals are converted into 8-bit symbol-rate digital signals and then passed to a fully digital decision-feedback equalizer (DFE) having two feedforward taps and one feedback tap. The equalizer also employs 8-bit tap-weights and internal arithmetic. Some more details on the equalizer and its adaptation algorithm can be found in [20]. Timing recovery is carried out using a zero-crossing type PD. The carrier recovery loop is a polarity-type DFL, the VCO control signal of which is derived from the equalizer output for more robustness against multipath fading and, more generally, against linear signal distortion [20]. The loop filter is of the phase lead-and-lag type, and the IF of the modem is 140 MHz. During the acquisition measurements, the equalizer adaptation algorithm was disabled so as to avoid interaction between the equalizer and the control signal of the carrier recovery loop. In this mode, the equalizer can be regarded as a pure delay, which naturally reduces the loop acquisition range.

Three PFD's were tested and compared to the original PD. In all of them, the windows are square shaped and correspond to $|e_k^I| < 0.5$ and $|e_k^Q| < 0.5$. The first PFD (referred to as frequency detector A) employs the 8 diagonal points, the second (frequency detector B) employs only the outer 4 diagonal points, and the third (frequency detector C), only the inner 4 diagonal points (see Fig. 7).

The mean acquisition time was measured with the three PFD's as well as with the original PD, and displayed as a function of the frequency offset. In doing these measurements, a low-frequency signal was used to periodically enable and disable (set to zero) the PD output. The frequency of this signal was adjusted to an appropriate value in the range of a few Hz to some fraction of a Hz depending on the acquisition time to be measured. A lock indicator was built which gives an accurate reading of the loop lock/unlock state. The delay between the two signals was then measured and averaged over a sufficient number of measurements to obtain a mean acquisition time.

B. The Results

The results obtained using the loop parameters

$$W_L = 107 \text{ kHz},$$

$$\tau_1 = 22 \text{ ms},$$

and

$$\zeta = 0.83$$

are summarized in Fig. 14. Clearly, the tested PFD's lead to a substantial increase of the acquisition range, the best performance being obtained with frequency detector A. For instance, if an acquisition time of less than 10 ms is required, the acquisition range is 120 kHz with the original PD, 1.4 MHz with frequency detector A, 800 kHz with frequency detector B, and 1.15 MHz with frequency detector C. Further, if an acquisition time of 100 ms is allowed, the acquisition range with the original PD remains smaller than 200 kHz, whereas it exceeds 3 MHz with frequency detector A. Thus, the acquisition range of the original PD is increased by more than an order of magnitude by the proposed PFD's.

It is not surprising to see that frequency detectors B and C did not perform as well as frequency detector A which uses more signal points. Furthermore, frequency detector C performed better than frequency detector B, although the SNR is higher for the outer than for the inner diagonal states. This must be attributed to the fact that windows of equal size lead to a larger phase angle for the inner diagonal points than for the outer diagonal points.

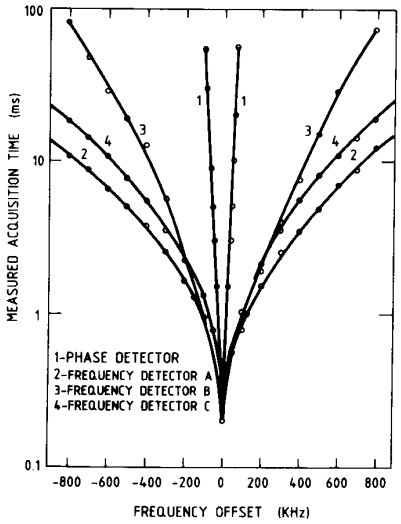

Fig. 14. Measured acquisition time versus frequency offset using a 16 QAM laboratory modem and three PFD's.

VI. Steady-State Performance

Due to the small noise bandwidth of the carrier recovery loop, the magnitude of the instantaneous phase error in the steady-state exceeds θ with a very small probability. Consequently, in PSK systems, the steady-state jitter performance of the presented PFD's is virtually identical to that of the original PD. The situation is, however, different in QAM systems. All the signal states are not used for phase information extraction, and this must lead to an increase of the phase jitter with respect to the original PD. This is indeed the case, and will be proven here assuming that the signal is corrupted only by an additive white Gaussian noise.

The noise samples being uncorrelated, it is easily established that successive PD outputs are also uncorrelated, i.e.,

$$E(\epsilon_k \epsilon_{k+l}) = 0 \text{ for } l \neq 0. \tag{12}$$

Utilizing (11) and (12), we obtain for the PFD output correlation function

$$E(u_k u_{k+l}) = p^l E(u_k^2) = p^l E(\epsilon_k^2) \tag{13}$$

with p = prob $(r_k \notin \mathfrak{D})$. In the steady state, p is essentially the same as the probability of transmitting a signal state that is discarded by the PFD. For PSK systems we have $p = 0$, but for frequency detector A described in the previous section for 16 QAM we have $p = 1/2$, and for frequency detectors B and C employing only 4 diagonal points, $p = 3/4$.

The noise spectral density within the loop bandwidth is easily evaluated as follows:

$$S_0 = \left[E(u_k^2) + 2 \sum_{l=1}^{\infty} E(u_k u_{k+l}) \right] T. \tag{14}$$

Now, utilizing (13) in (14), it follows that

$$S_0 = T \left[1 + 2 \sum_{l=1}^{\infty} p^l \right] E(\epsilon_k^2)$$

$$= T \frac{1+p}{1-p} E(\epsilon_k^2). \tag{15}$$

The next step is to evaluate the PD gain K_d and the two-sided loop noise bandwidth W_L because the steady-state jitter variance is given by [5]

$$\sigma_\varphi^2 = \frac{W_L S_0}{K_d^2} . \tag{16}$$

For the second-order loops considered, W_L is well approximated as

$$W_L \simeq \frac{K_0 K_d F_0 \tau_2 + 1}{2\tau_2} . \tag{17}$$

For the polarity-type PD at hand, it is easily verified that frequency detector A does not alter the detector gain (the mean power of the diagonal points in 16 QAM is the same as the mean power of the whole signal constellation), whereas frequency detector B multiplies it by 3/2 and frequency detector C by 1/2. The increase of the loop bandwidth is, in contrast, a function of the loop parameters. The results obtained using the loop parameters

$$K_0 T = 0.784$$

$$F_0 = 8 \times 10^{-4}$$

and

$$T/\tau_1 = 1.82 \times 10^{-6}$$

in 16 QAM are reported in Table I. This table shows, for two SNR's and for each of the three considered PFD's, the ratio of the phase jitter's root mean square (rms) value with respect to that of the original PD. It can be noticed that the theoretical results are in very close agreement with the results obtained from Monte-Carlo simulations.

Clearly, the phase noise considerably increases, particularly in the case of frequency detector C. Similar results were also obtained experimentally in the laboratory. To avoid such an increase of the phase jitter in QAM systems, one must switch back to the original PD as soon as carrier lock is acquired. This strategy benefits from both fast carrier acquisition over an extended frequency range, and small steady-state phase jitter. To accomplish this, a lock indicator is needed, and as soon as lock is acquired, the control logic in Fig. 8 is disabled and a logic 1 is set at its output, so that every PD output is passed to the VCO (through the loop filter) irrespective of the I and the Q coordinates of the instantaneous signal sample. The same strategy was also suggested in [19] to combine the improved acquisition properties of the "selective-gated" loop and the reduced jitter provided by the original loop that employs all the points of the signal constellation.

TABLE I
THEORETICAL AND SIMULATED FACTORS OF INCREASE OF THE PHASE JITTER RMS VALUE IN 16 QAM FOR THE THREE PFD'S A, B, AND C

	THEORETICAL			SIMULATED		
SNR	A	B	C	A	B	C
20 dB	1.73	2.08	4.10	1.73	2.21	4.04
40 dB	1.73	2.15	3.74	1.73	2.30	3.59

VII. Conclusions

We have presented a new class of PFD's for fast carrier recovery in digital communication systems. The key idea behind these detectors is applicable to a large variety of modulation schemes, and particularly suitable for the popular PSK and (rectangular) QAM signal formats. By means of computer simulations and laboratory experiments, the new PFD's were shown to improve dramatically the loop acquisition properties. In PSK carrier recovery, this improvement is achieved with no penalty in phase jitter performance. In QAM systems, due to the use of some diagonal points only, the phase jitter is increased, but this is easily avoided by switching the control mode back to the original PD after lock is acquired. The new PFD's require very small additional circuitry with respect to conventional PD's, and are easily implemented at high data rates. The considerably large acquisition range achieved makes these detectors very attractive for digital microwave radio systems and other applications requiring carrier recovery loops that must cope with large frequency offsets.

A final remark to make at this point is that all the computer simulations and laboratory experiments we have reported were done in a distortion-free environment. A natural question is how the new PFD's perform in the presence of multipath fading, which is a major cause of outage in digital microwave radio. Although it may be expected that multipath fading reduces the frequency range over which the loop has an FD characteristic, as well as the FD gain over that range, the new detectors should keep a considerable advantage over conventional PD's in that environment.

Acknowledgment

The authors are indebted to their former colleague L. Desperben for her major contributions to the early stages of the work presented in this paper.

References

[1] Y. Takeda *et al.*, "Performance of 256QAM modem for digital radio systems," in *Proc. GLOBECOM'85 Conf. Rec.*, vol. 3, New Orleans, LA, Dec. 1985, pp. 1455–1459.
[2] Y. Yoshida *et al.*, "6 GHz 140 Mbps digital radio repeater with 256QAM modulation," in *Proc. ICC'86 Conf. Rec.*, vol. 3, Toronto, Ont., Canada, June 1986, pp. 1482–1486.
[3] W. C. Lindsey, *Synchronization Systems in Communications and Control.* Englewood Cliffs, NJ: Prentice-Hall, 1972.
[4] B. S. Glance, "New phase-lock loop circuit providing very fast acquisition time," *IEEE Trans. Microwave Theory Technol.*, vol. MTT-23, pp. 747–754, Sept. 1985.
[5] F. M. Gardner, *Phaselock Techniques.* New York: Wiley, 1979.
[6] D. G. Messerschmitt, "Frequency detectors for PLL acquisition in timing and carrier recovery," *IEEE Trans. Commun.*, vol. COM-27, pp. 1288–1295, Sept. 1979.
[7] J. A. Bellisio, "A new phase-locked timing recovery method for digital regenerators," in *Proc. ICC'76 Conf. Rec.*, vol. 1, June 1976, pp. 10–17.
[8] C. R. Cahn, "Improving frequency acquisition of a Costas loop," *IEEE Trans. Commun.*, vol. COM-25, pp. 1453–1459, Dec. 1977.
[9] D. Richman, "Color carrier reference phase synchronization accuracy in NTSC color television," *Proc. IRE*, vol. 12, pp. 106–133, Jan. 1954.
[10] F. M. Gardner, "Properties of frequency difference detectors," *IEEE Trans. Commun.*, vol. COM-33, pp. 131–138, Feb. 1985.
[11] P. Vandamme, G. Verdot, and A. Leclert, French pat. 83 15794, Oct. 1983.
[12] F. D. Natali, "AFC tracking algorithms," *IEEE Trans. Commun.*, vol. COM-32, pp. 935–947, Aug. 1984.
[13] H. Sari, L. Desperben, and S. Moridi, "A new class of frequency detectors for carrier recovery in QAM systems," in *Proc. ICC'86 Conf. Rec.*, vol. 1, Toronto, Ont., Canada, pp. 482–486, June 1986.
[14] M. K. Simon and J. G. Smith, "Carrier synchronization and detection of QASK signal sets," *IEEE Trans. Commun.*, vol. COM-22, pp. 98–106, Feb. 1974.
[15] A. Leclert and P. Vandamme, "Universal carrier recovery loop for QASK and PSK signal sets," *IEEE Trans. Commun.*, vol. COM-31, pp. 130–136, Jan. 1983.
[16] S. Moridi and H. Sari, "Analysis of four decision-feedback carrier recovery loops in the presence of intersymbol interference," *IEEE Trans. Commun.*, vol. COM-33, pp. 543–550, June 1985.
[17] I. Horikawa, T. Murase, and Y. Saito, "Design and performance of a 200 Mbit/s 16QAM digital radio system," *IEEE Trans. Commun.*, vol. COM-27, pp. 1953–1958, Dec. 1979.

[18] I. Horikawa and Y. Saito, "16 QAM carrier recovery with selective gated phase-locked loop," *Trans. IECE Japan,* vol. 63-B, pp. 692-699, 1980.

[19] H. Matsue and Y. Saito, "Characteristics of a 16 QAM carrier recovery phase locked loop with control mode selection function," *Trans. IECE Japan,* vol. J68-B, pp. 387-394, 1985.

[20] H. Sari, S. Moridi, L. Desperben, and P. Vandamme, "Interaction between an adaptive equalizer and a decision-feedback carrier recovery loop," in *Digital Communications,* E. Biglieri and G. Prati, Eds. Amsterdam, The Netherlands: Elsevier, 1986.

★

Hikmet Sari (S'78-M'81) was born in Antakya, Hatay, Turkey, on February 1, 1954. He received the Dipl. Eng. and the Dr. Eng. degrees in electrical engineering from the Ecole Nationale Supérieure des Télécommunications (ENST), Paris, France, in 1978 and 1980, respectively.

Since 1978, he has been with the Laboratoires d'Electronique et de Physique Appliquée (LEP, a member of the Philips Research organization), Limeil-Brévannes, France. As a research scholar from 1978 to 1980, he worked towards his doctorate on adaptive filtering. He became a member of the Technical Staff of LEP in 1980, and until 1987, he conducted research in digital microwave radio systems with a particular emphasis on bandwidth-efficient modulation techniques, timing and carrier synchronization, and adaptive channel equalization. During a part of this period, he was also involved in research on adaptive modems for digital HF communications. He has extensively published, and holds several patents issued or pending in these fields. In September 1987, he was appointed Head of the newly created Signal Acquisition and Processing Division of LEP. Presently, he also holds the rank of "Professeur Associé" at ENST, where he participates in the Postgraduate Research Commission, and teaches graduate-level courses in digital communications. His current research interests are in the areas of communication theory, digital communications, the theory and the applications of adaptive filtering, and digital signal processing.

Dr. Sari is currently serving as Editor for Channel Equalization of the IEEE TRANSACTIONS ON COMMUNICATIONS. He is a member of several Technical Committees of the IEEE Communications Society.

★

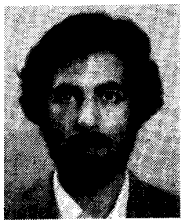

Said Moridi was born in Iran in 1957. He received the Engineering degree from the Ecole Nationale Supérieure des Télécommunications, Paris, France, in 1980, and the Diplôme d'Etudes Approfondies in probability theory from the Université Pierre et Marie Curie, Paris, France, in 1981.

Since 1981, he has been with the Laboratoires d'Electronique et de Physique Appliquée, Limeil-Brévannes, France. His current research interests include synchronization systems, digital communications, bandwidth-efficient modulations, and adaptive filtering in digital microwave radio systems and HF communications.